CHANCE project

(Contract Number: 755371)

Report on study of the release behaviour of radiocarbon from irradiated graphite waste using CRDS

DELIVERABLE (D5.4)

Work Package 5

Author(s): **Johannes Lehmuskoski, Guillaume Genoud, Antonietta Rizzo, Alberto Ubaldini, Chiara Telloli**

Reporting period 1: 01/06/2020– 31/03/2022

Date of issue of this report: **29.3.2022**

Start date of project: **01/06/2017** Duration: 58 Months

This project has received funding from the Euratom research and training programme 2014-2018 under grant agreement No 755371;		
Dissemination Level		
PU	Public	X
CO	Confidential, only for partners of the CHANCE project and EC	

History chart			
Status	**Type of revision**	**Partner**	**Date**
Draft	Initial version	VTT	16.3.2022
Final	Second version	VTT	29.3.2022

Reviewed by

Andra

Approved by

The Executive Board

Contents

Table of tables

1. Objectives and Introduction

The CHANCE project aims to address the specific issue of the characterization of conditioned radioactive waste. The characterization of fully or partly conditioned radioactive waste is a specific issue because unlike for raw waste, its characterization is more complex and therefore requires more advanced non-destructive techniques and methodologies.

The first objective of the CHANCE project is to establish at the European level a comprehensive understanding of current conditioned radioactive waste characterization and quality control schemes across the variety of different national radioactive waste management programmes, based on inputs from end-users members such as Waste Management Organizations and storage operators.

The second objective of CHANCE is to further develop, test and validate techniques already identified that will improve the characterization of conditioned radioactive waste, namely those that cannot easily be dealt with using conventional methods. Specifically, the work on conditioned radioactive waste characterization technology will focus on:

- Calorimetry as an innovative non-destructive technique to reduce uncertainties on the inventory of radionuclides;
- Muon Tomography to address the specific issue of non-destructive control of the content of large volume nuclear waste;
- Cavity Ring-Down Spectroscopy (CRDS) as an innovative technique to characterize outgassing of radioactive waste.

The present report focuses on activities from Work Package 5 related to the development of the CRDS for the detection of radioactive gases. The focus of the Task 5.2 was particularly in characterisation of outgassing of radiocarbon from graphite waste and experiment novel spectroscopy technique known as cavity ring-down spectroscopy (CRDS) for the detection. The nature of radiocarbon migration in irradiated graphite and outgassing in different environmental conditions were also investigated.

Nuclear graphite grades share common properties in terms of original isotopic composition of carbon and the material structure, which constitutes of graphene layers with different orders of organisation. The basic elements of the structure are quasi-perfect stacks of graphene layers, which are combined together with varying orientations. The combination of graphene stacks defines nanostructure and microstructure of graphite, which results in complex spatial arrangement of graphitised grains and binder and filler particles confining inter-granular pores [1,2]. Typically, the overall porosity of nuclear graphite is between 14% and 24 % [3,4], but irradiation can increase it substantially [2,5]. The isotopic composition of graphitic carbon is the same as for the carbon generally in the nature, which is composed of the ^{12}C isotope with about 1 % of ^{13}C, and negligeable amount of ^{14}C (~ppt).

Irradiation of graphite forms ^{14}C due to thermal neutrons reacting with ^{14}N and ^{13}C in $^{14}N(n,p)^{14}C$ and $^{13}C(n,\gamma)^{14}C$ reactions [4]. Nitrogen is a gaseous impurity that is present in the graphite pores and subsequently, the ^{14}C produced from nitrogen is usually not covalently bound to the graphite matrix and thus can be released from the graphite during reactor operation because of radiation induced corrosion[5,6]. ^{13}C instead, is part of the pristine graphite matrix, as this isotope makes up one percent of the natural carbon, and the ^{14}C produced remains linked in the graphite structure. In ^{14}C production, the neutron capture cross-section for ^{14}N is 1.8 barns, while it is 0.0015 barns for ^{13}C, and therefore the nitrogen originating radiocarbon is typically dominant [7]. However, the concentration of nitrogen in the pores of graphite varies depending on the way of production and amount of irradiation on the graphite [5,6]. The origin of the ^{14}C in graphite affects the outgassing, but there is no information about the rate of outgassing of ^{14}C in graphite due the lack of techniques to measure it. Therefore, development of new methods such as the CRDS is important to enable safe handling and effective storage of the radiocarbon containing waste.

2. Methods

2.1 Radiocarbon detection with cavity ring-down spectroscope

The detection of radiocarbon (^{14}C) outgassing was based on the detection of $^{14}CO_2$ molecule P(20) absorption line at mid-infrared at 2209.109 cm^{-1}. The low absorption of the line because of low concentration of the $^{14}CO_2$ in the samples required using cavity ring-down spectroscopy to measure the concentration. Cavity ring-down spectroscopy is based on measuring decay time of light intensity between two high reflectivity mirrors. A laser light is coupled into a cavity formed by the two mirrors, resulting in light intensity build-up in the cavity. When light is switched off, the light intensity decays out exponentially, because of the loses in the mirrors. A gas, which absorbs light at the laser wavelength, results in a faster decay than in an empty cavity. The wavenumber dependent absorption coefficient at the measured wavelength can be calculated using the following equation: $\alpha(\nu) = 1/[c\tau(\nu)] - 1/[c\tau_0]$, where ν is the wavenumber and c is the speed of light. τ is the decay time of the exponential decay, known as the ring-down time, measured with sample in the cavity and τ_0 is the ring-down time in an empty cavity. Using the cavity ring-down spectroscopy, the optical pathlength in the gas can be maximised, which allows detection of even the lowest gas concentrations.

The cavity ring-down setup is shown in the Figure 1, and further details can be found in Ref [8]. In the setup, a L12004-2209H-C quantum cascade laser (QCL) from Hamamatsu with a central wavelength at 4.527 μm was used. The laser is guided through collimating lens, two optical isolators and two mode-matching mirrors to an optical cavity formed by two high-reflectivity ZnSe mirrors. The high-reflectivity mirrors have reflectivity of 99.97 % and 1 metre radius of curvature. The second mirror is

mounted on a piezo-electric actuator-controlled platform. The cavity and the mirrors are enclosed inside an insulated and temperature-controlled cell, which has antireflective-coated CaF_2 windows for the laser entrance and exit. The low pressure required by the measurements is achieved with a scroll pump and the pressure is monitored with capacitance manometer. After the second mirror the light is guided to a photovoltaic detector and the detector signal is recorded by a FPGA card. The signal is processed and analysed with a LabVIEW-based software. By simultaneously scanning the cavity length with the mirror on the piezo mount, and scanning the laser wavelength, an absorption spectrum of the scanned laser range is formed. The spectroscope is positioned to a moveable 19-inch instrument rack.

The concentration of the radiocarbon was determined by fitting a sum of Voigt profiles with a non-linear least-square fitting routine to the measured absorption spectra, which were first smoothed with a moving-average filter. To obtain the radiocarbon concentration, the total CO_2 concentration in the cavity needed to be measured. This was done by measuring a $^{13}CO_2$ line at 2209.77 cm^{-1} with the CRDS and using the same line fitting method as for the radiocarbon spectra. The concentration of i = C14 or i = CO_2 is calculated from the absorption line area using equation: $C_i = (A_i k_b T)/(S_{oi} p)$, where A_i is the absorption line area, k_b is the Boltzmann constant, T is the sample temperature, S_{oi} is the absorption line strength and p is the sample pressure. The $^{14}C/^{12}C$ concentration was calculated as C_{C14}/C_{CO2} ratio.

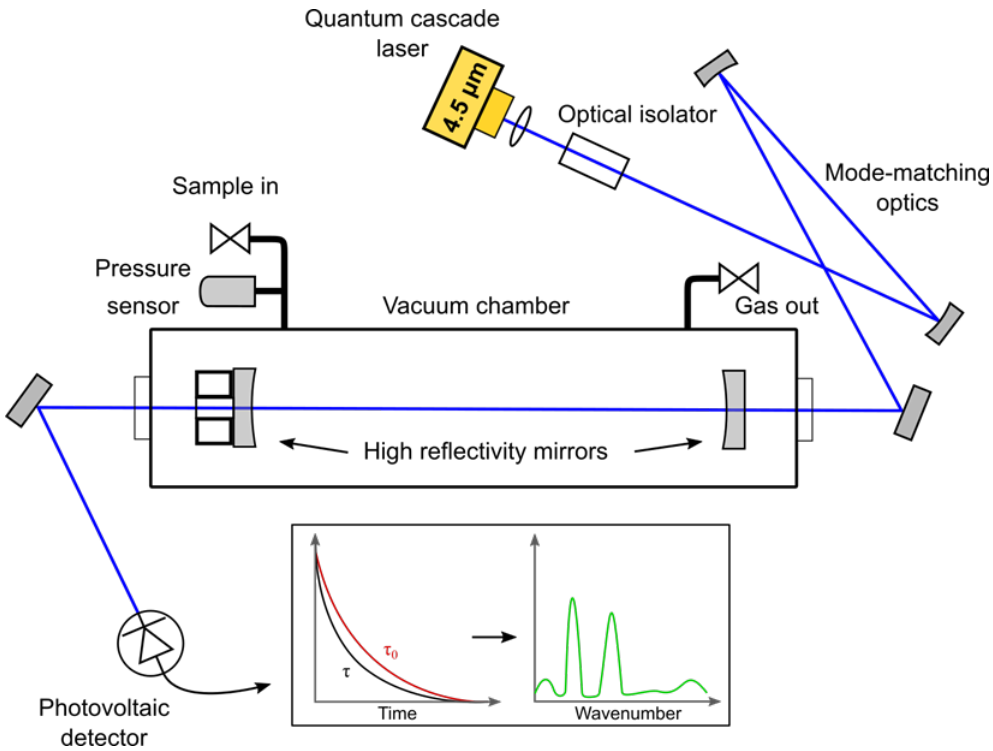

Figure 1. Schematic of the CRDS arrangement used for ^{14}C outgassing measurements.

2.2 Sample processing unit

The CRDS measurement requires concentrating the CO_2 to enable detection of low ^{14}C concentrations at good accuracy. Therefore, an on-line sample processing unit was built for the CO_2 purification and used together with the CRDS. The sample processing unit is shown in Figure 2, and detailed information of the sample processing unit is given in Ref [8].

The sample processing unit takes in samples in gas phase. A diaphragm pump is used to flow the air through the sample processing unit. The gas flows through a particle filter to a catalyser, which converts methane and other hydrocarbons to CO_2. The conversion occurs on palladium catalyst which is kept at 500 °C temperature. The preparation of catalyst is presented in more detail in Ref [9]. Conversion of hydrocarbons to CO_2 allows detecting ^{14}C also originally present in other molecular species than CO_2 (organic molecules such as methane). The catalyser can also be bypassed to get the ^{14}C content only in CO_2. After the catalyser, a Vaisala GMP343 carbon dioxide sensor is used together with a pressure sensor to detect the CO_2 content in the sample air. A mass flow controller adjusts the flow speed, and solenoid valves guide the sample flow to one of two identical CO_2 traps. The two traps are used sequentially so, that when one trap is releasing trapped CO_2, the sample air is flown through the other trap that collects new CO_2 sample. The traps are made of aluminium blocks made into form of heat sinks. The trapping material, Lewatit VP OC 1065 ion-exchange resin from Lanxess, is positioned inside a drill hole made into the blocks. The resin adsorbs CO_2 selectively from air at room temperature. The CO_2 is released to the CRDS cell from the resin by heating the trap over 50 °C temperature. The heating is achieved with resistive heaters. After the CO_2 release, the trap is cooled back to room temperature with fans. The trapping time depends on the CO_2 concentration of the sample air, but typically 30 minutes was the minimum time to gather enough CO_2 for the CRDS measurement.

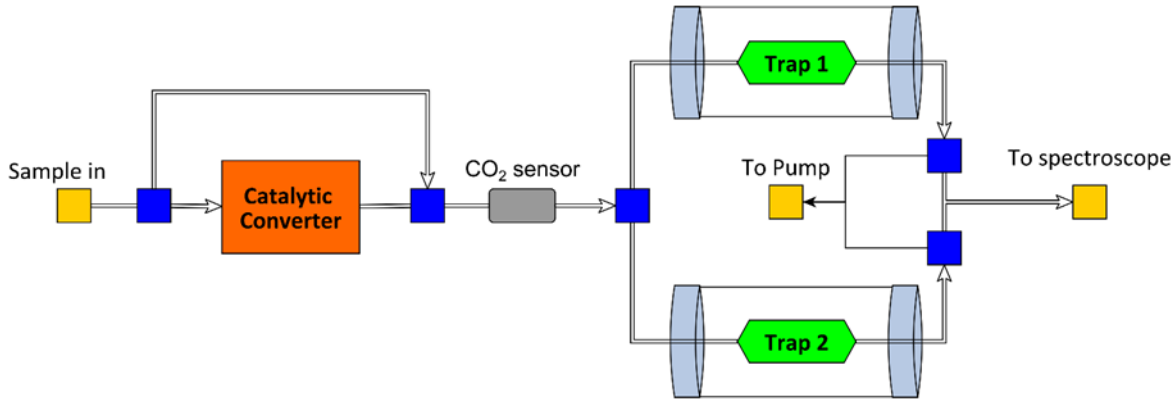

Figure 2. Sample processing unit.

2.3 Gas sample recovery from sealed graphite crates

Gas samples were collected from four sealed steel crates containing graphite from the thermal column of FiR1 research reactor. The research reactor was disassembled in 1995 and the graphite in the steel crates was stored in research wells in VTT laboratories. Small amounts of other materials such as plastic and metal were stored in the crates together with the graphite as is visible in a photo of one of the crates in Figure 3. The crates were labelled as crate 101, 102, 103 and 104. Crate 101 was opened in 2011 for sample collection and sealed again. C14 activities of graphite in the crates were estimated based on $^{14}C/^{152}Eu = 0.4$ activity ratio reported in Ref [4,10]. Measured ^{152}Eu activities and calculated ^{14}C activities in the graphite are shown in the Table 1.

Table 1. Measured ^{152}Eu activities and corresponding ^{14}C activities.

crate	Measured ^{152}Eu activity (MBq)	^{14}C activity calculated from ^{152}Eu (MBq)
101	375	150
102	222	89
103	739	296
104	539	248

The gas samples were collected in July 2019 into 50 litre gas cylinders, which were evacuated to vacuum prior the collection. Before opening the crates for other research purposes, the air from the crates was taken through a bolt hole with a 6 mm diameter PFA tubing with a particle filter, employing the vacuum in the cylinder as the gas flow driving force. The bolt hole around the tube was blocked with a hand in a rubber clove. Mixing of room air to the sample air was considered minor, as approximately 1 metre of the sampling tube could be put inside the crate prior sample acquisition. In addition, the gas volume inside the crates was multiple times the volume of sample taken to the gas cylinders, which prevented formation of large pressure difference between the room air and air inside the crate. The gas cylinders were filled to atmospheric pressure and labelled according to the labelling of the crates.

Figure 3. Sealing the graphite container crate. Some of the graphite blocks had additional plastic packaging inside the crates.

2.4 Gas sample measurements with CRDS

The samples from the gas cylinders were measured using the sample processing unit together with the CRDS as shown in Figure 4. The measurements were conducted so that the gas from a sample cylinder was flown through the sample processing unit, and after sufficient trapping time, the CO_2 was released to the CRDS for ^{14}C detection. Suitable flow settings were determined by making measurements with a 50-litre gas cylinder containing room air. Flowing the air from the gas cylinder with a mass flow controller setting at 0.50 l/min for 40 minutes and releasing the trapped CO_2 to evacuated CRDS cavity resulted in about 5 mbar pressure in the cavity, which was sufficient for the CRDS measurement. For each cylinder, measurements were done to measure the total ^{14}C and to measure ^{14}C that was originally in the form of CO_2. This required trapping two samples with the sample processing unit: first one trapping with catalyst, and second one without, and measuring them separately in the CRDS.

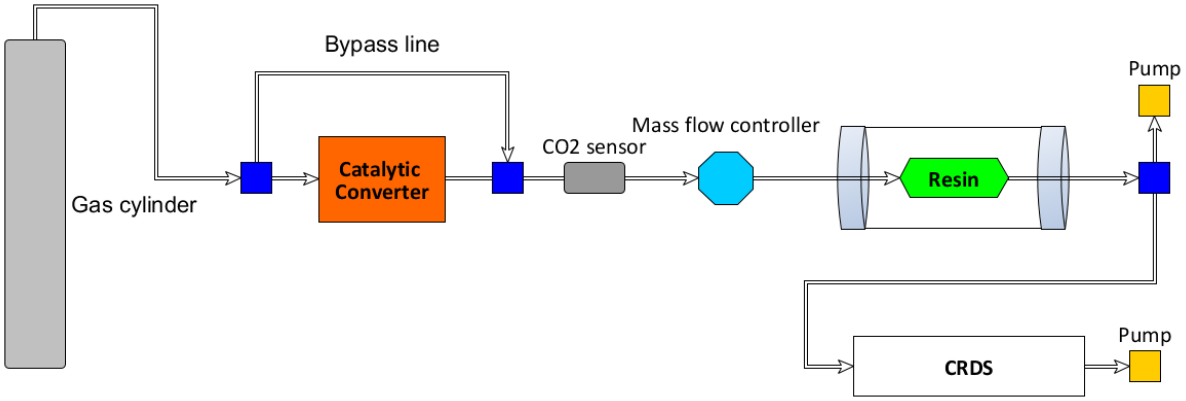

Figure 4. Measurement schematics with gas cylinder. The gas flow from the gas cylinder was controlled with a regulator and a needle valve at the cylinder output (not visible in the sketch).

2.5 Pyrolyser measurements of graphite samples

C14 activity of irradiated graphite was measured using a pyrolyser coupled with the sample processing unit and the CRDS. The graphite samples were collected from the FiR1 thermal column graphite from the surface of the graphite blocks consisting of small cylindrical pellets, from which small pieces were cut out with a surgeon knife. Photo of sample #5 is shown in Figure 5, as an example. From the few grams of sample, 13 – 42 mg of graphite was taken for individual C-14 measurements with the CRDS setup. The measurements were done in September 2020.

A Catalytic Pyrolyser-2Trio from Raddec International was used to convert the graphite samples to carbon dioxide. The produced carbon dioxide was flown through and trapped with the sample processing unit and released to the CRDS for C-14 detection, as shown in the schematics in Figure 6. The pyrolyser has two sample zones in serries followed by an oxidising catalyser. The catalyser contains 0.5 % platina-alumina pelletised catalyst, which is heated to 800 °C. The graphite samples were loaded on silica-glass boats and positioned in the sample zone 1, which is the first sample zone after the air inlet to a silica-glass tube enclosing the sample zones and the catalyser. In the measurements, sample zone temperatures of 20 – 800 °C were used. A synthetic air cylinder was connected to the pyrolyser air inlet to feed in CO_2-free air. After first graphite combustion tests, a suitable synthetic air mass flow of 0.40 l/min at the sample processing unit mass flow controlled was adjusted for the experiments. Based on the first combustion tests, a heating sequence for the measurements was programmed to the pyrolyser. In the heating program, the pyrolyser heats the zone 1 from room temperature to 500 °C gradually in 35 minutes. This is followed by 5 minutes period, when the temperature is not changed. When zone 1 reaches 500 °C, it moves automatically in zone 2. During this time, the CO_2 trapping flow in the sample processing unit is switched to the other trap. After the stop, the heating is continued gradually for 35 minutes to 800 °C. The 800 °C is maintained until the CO_2 output from the sample in the pyrolyser decreases, which meant that all the sample was combusted.

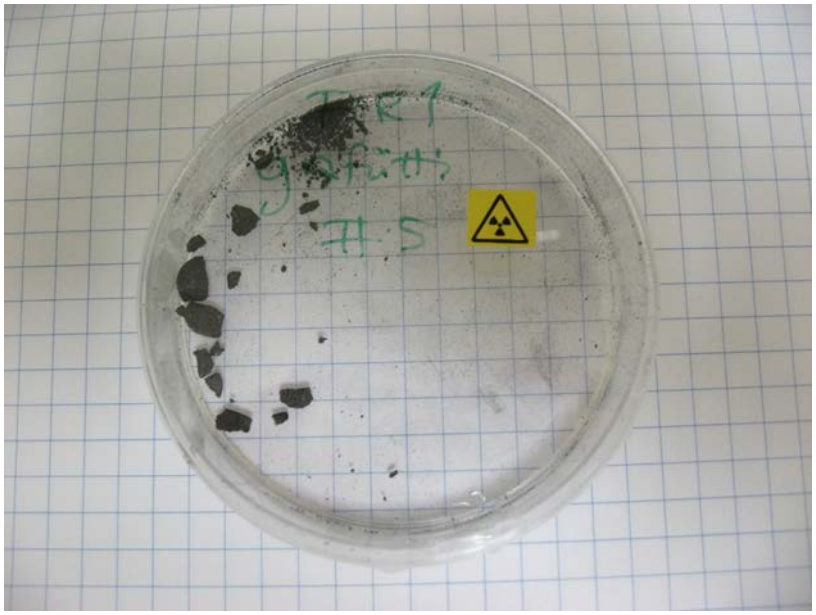

Figure 5. Pieces of graphite cut out from graphite pellets. In the pyrolyser experiments, typically only the smaller graphite pieces were used as samples.

In later measurements, lower temperatures of 650 – 680 °C were used to experiment the rate of CO_2 outgassing at different temperatures. Temperature steps of 10 °C were also used to see the effect of raising temperatures in the outgassing.

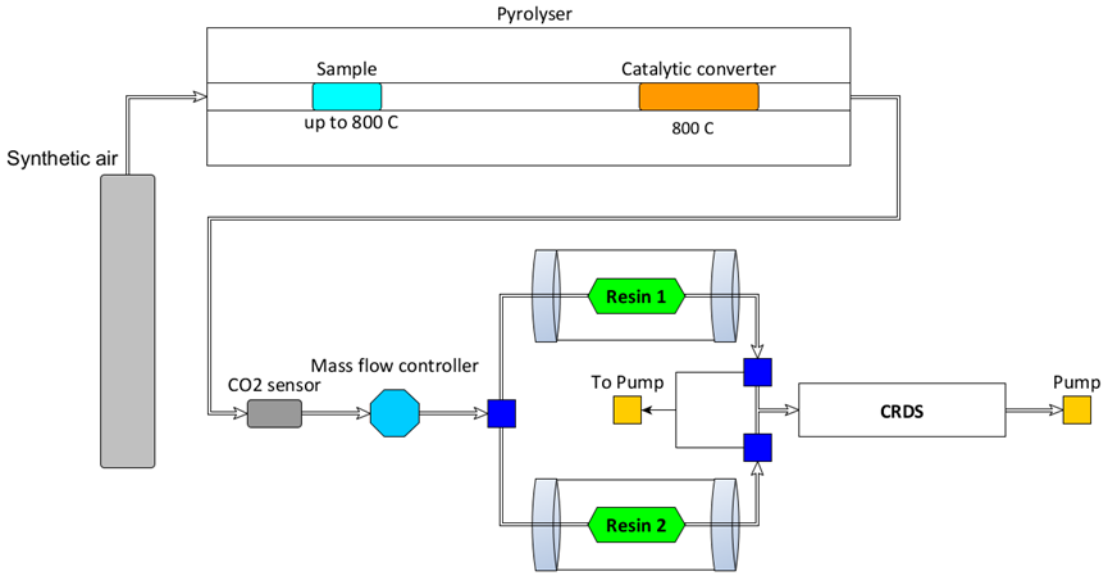

Figure 6. Schematics of pyrolyser experiments. The air flow through the system was controller with a regulator and a needle valve at the synthetic air cylinder outlet and the mass flow controller in the sample processing unit. The catalytic converter of the sample processing unit was bypassed to reduce flow resistance in the system.

3. Results

3.1 Graphite crate gas measurements

The measurements of the gas cylinder samples were started from cylinders 102 and 104. The gas cylinder pressure dropped during the trapping for total ^{14}C measurement from 1 bar to ~ 0.6 bar, which also caused the mass flow speed during the trapping to fall, being in the end of the trapping about 0.3 l/min. For the second trapping for the ^{14}C originally in the form of $^{14}CO_2$, the mass flow recovered in the beginning to 0.4 l/min, probably because of equalising of the pressures in the sample processing unit gas lines, before it started to fall again to 0.3 l/min. To ensure sufficient trapping of CO_2 in the second measurements, the trapping times for total ^{14}C from cylinders 101 and 103 were reduced to 30 minutes. 30 minutes trapping time was used also for all measurements of the ^{14}C originally in the form of $^{14}CO_2$.

The results of the trapping are listed on Table 2. From the CO_2 concentrations, it is evident that samples 101 and 104 had notable portion of carbon species in the form of hydrocarbons in addition to carbon dioxide. In sample 104, the hydrocarbons contained over one quarter of the carbon in the sample air. The CO_2 concentration in the sampled air affected the final CO_2 pressure released to the CRDS cavity more than the trapping time.

Table 2. Results of CO_2 trapping of the graphite crate gases.

Sample	Measurement	CO_2 concentration in sample air	Trapping time	CO_2 pressure released to CRDS
		ppm	min	mbar
101	^{14}C Total	480	30	5.47
	^{14}C in CO_2	430	30	5.33
102	^{14}C Total	395	40	4.59
	^{14}C in CO_2	380	30	3.87
103	^{14}C Total	398	30	4.82
	^{14}C in CO_2	397	30	4.73
104	^{14}C Total	585	40	6.10
	^{14}C in CO_2	430	30	5.48

For the ^{14}C activity concentrations measurements, the pressure in the cavity needed to be reduced as the ^{14}C concentrations in most of the samples were high: between 1200 Bq/m^3 – 7000 Bq/m^3. Only in sample 102 the ^{14}C activity concentration was found low enough: 130 ± 40 Bq/m^3, to be measured in the pressure of the CO_2 release from the trap. The other samples were measured after pumping down the CRDS cavity pressure to 1.5 or 2.0 mbar to decrease the absorption due to otherwise too intensive $^{14}CO_2$ line. Absorption line fit to the absorption spectra of sample 103 total ^{14}C, and ^{14}C in CO_2 activity concentration measurements are shown in Figure 7.

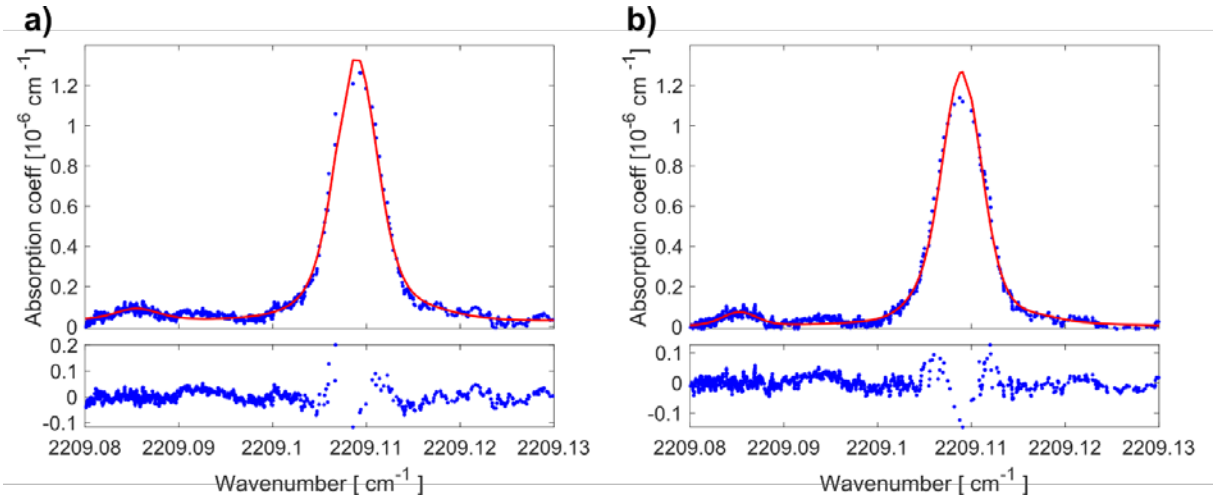

Figure 7. CRDS spectra with spectral line fit: **a)** total ^{14}C activity concentration in the sample 103 which was 5030 ± 900 Bq/m^3; **b)** ^{14}C activity concentration originally in CO_2 in the sample 103 which was 4380 ± 790 Bq/m^3.

The concentrations of all the ^{14}C activity concentration measurements from the gas cylinders are shown in the graph on the Figure 8. In all the measurements the ^{14}C activity concentration in CO_2 only is slightly smaller than in all carbon species combined, even though the difference is within the error bars. The other carbon species with the higher ^{14}C activity concentration in the sample air are hydrocarbons and possibly some carbon monoxide. The ^{14}C activity concentration in CO_2 in sample 102 could not be measured, because of the low CO_2 concentration in the sample and low pressure in the trapping, which caused low CO_2 amount released to the CRDS cavity. The low pressure during the trapping resulted also to larger concentration of N_2O desorbed during the CO_2 release to the cavity, which resulted in higher background in the CRDS measurement. Therefore, an absorption line fit was not possible to the $^{14}CO_2$ peak. Such situation can be avoided in the future by using the 30 minutes trapping time for the earlier total ^{14}C measurement as was done for the samples measured after sample 102. All the other samples could be measured normally. The $^{14}C/^{12}C$ concentrations in hydrocarbons were calculated for samples 101 and 104 based on the difference in measured CO_2 concentrations in the trapped gas in the ^{14}C Tot and ^{14}C in CO_2 measurements, and on the $^{14}C/^{12}C$ concentrations in those measurements. The results for samples 101 and 104 are shown in the Figure 9. For sample 103, the difference in CO_2 concentrations

was only 1 ppm as shown in Table 2. It is also the measurement uncertainty, which is why the ^{14}C activity concentration was not reasonable to count. In sample 101, hydrocarbons had higher $^{14}C/^{12}C$ concentration than CO_2. In sample 104, CO_2 had higher $^{14}C/^{12}C$ concentration than hydrocarbons.

The CRDS measurements gave valuable information of the behaviour of ^{14}C in the gaseous form in the stored graphite samples. The outgassing of ^{14}C from irradiated graphite had not been studied before in such accuracy. The measurements showed that significant amount of ^{14}C is released in the air during storage of graphite. The measured ^{14}C activity concentrations from the air sampled from the storage crates mostly followed the ^{14}C activities calculated based on the ^{152}Eu measurements. Only the order of the most active crates based on the ^{152}Eu measurements was different than with the CRDS measurements from the air. However, the difference can be due to the rate of mixing of different carbon containing gases from the graphite to the air. The ^{14}C distribution in different molecular species was also studied, and the measurements showed that there were differences in the distribution between the samples. However, CO_2 is the most abundant airborne carbon species in the samples (74 – ~99 % of all carbon), and therefore contains most of the ^{14}C in the sampled air.

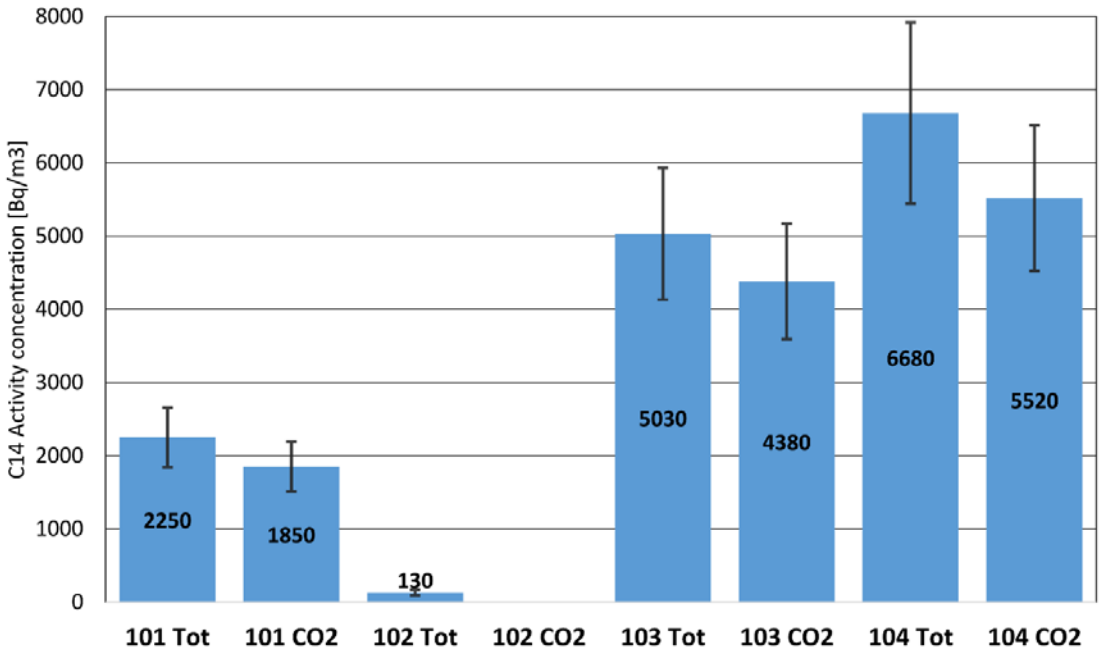

Figure 8. The measured ^{14}C activity concentrations in the graphite crate gases. In the horizontal axis, the values are labelled as the crate number followed by 'Tot' or 'CO_2', 'Tot' marking the total ^{14}C activity concentration in all carbon species, and 'CO_2' marking ^{14}C activity concentration in CO_2 only. The detected ^{14}C activity concentration values in Bq/m^3 are written in the columns. The error bars are shown in black on the column tops.

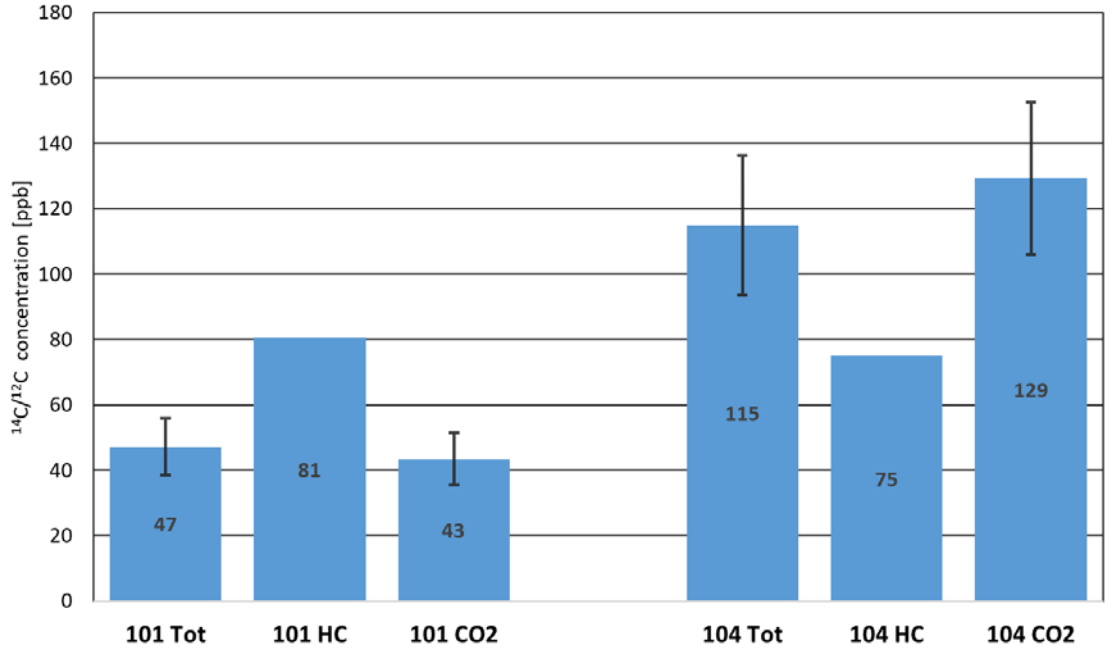

Figure 9. The $^{14}C/^{12}C$ concentrations in different carbon species. In addition to data in Figure 8, the HC in horizontal axis marks the ^{14}C activity concentration in hydrocarbons.

3.2 Pyrolyser graphite measurements

The measurements on the graphite pieces were started with total combustion of a sample, which was possible by heating the sample in the pyrolyser up to 800 °C. The first part of the heating program, from room temperature to 500 °C in 35 minutes, resulted to only small amount of CO_2 output from the sample. The CO_2 captured by the sample processing unit, and released after the trapping to the CRDS cavity, was insufficient to make a ^{14}C detection with CRDS. The second stage of the pyrolyser program: the heating from 500 °C to 800 °C in 35 minutes, resulted in clearly higher CO_2 output and allowed detection of ^{14}C with good accuracy. A graph showing the sample zone temperature and the CO_2 output as function of time is shown in Figure 10. Heating the graphite gradually results in exponentially growing CO_2 output, which reaches its maximum above 750 °C sample temperature. It is, however, possible that the maximum output occurs already at lower temperature, but because of the delay from the gas reaching the CO_2 sensor the CO_2 value is lagging behind. In the combustion measurement shown in Figure 10, the CO_2 reaches almost 20000 ppm. The maximum CO_2 output depended on the amount of graphite sample used in the combustion. From three graphite samples labelled: #1, #4 and #5, two or three samples of each were weighted, combusted, and measured with CRDS. The results are presented in Figure 11.

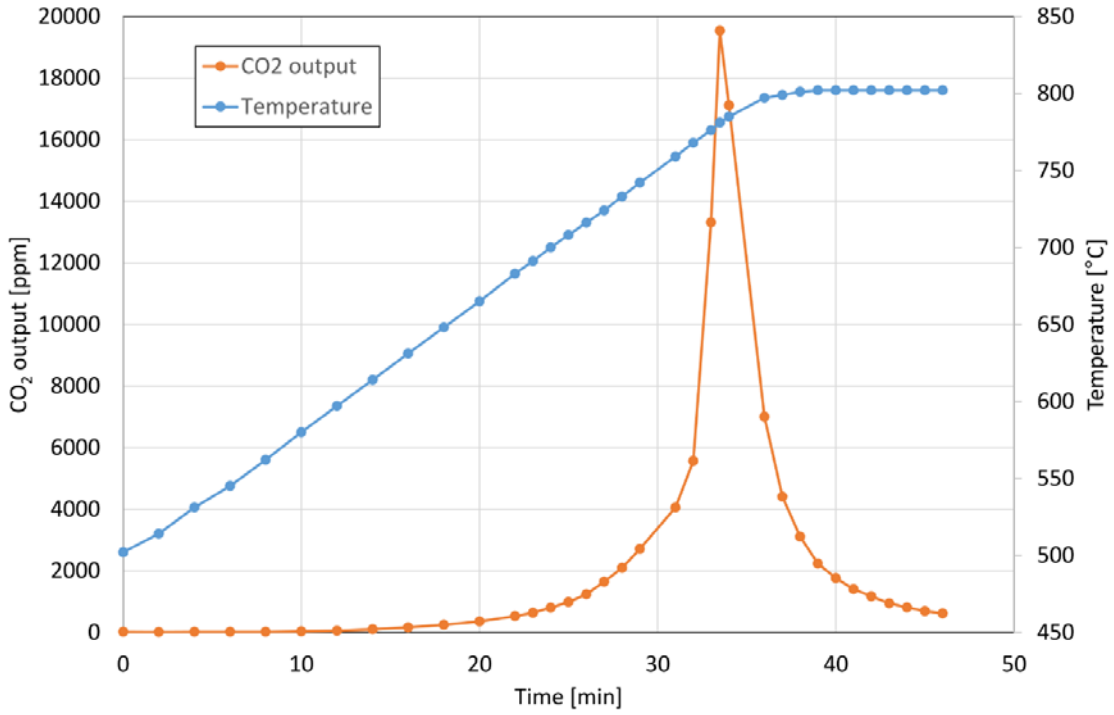

Figure 10. CO_2 output and sample temperature relation. Constant temperature gradient results in exponential CO_2 output above 700 °C, which ends quickly, when most of the sample is combusted.

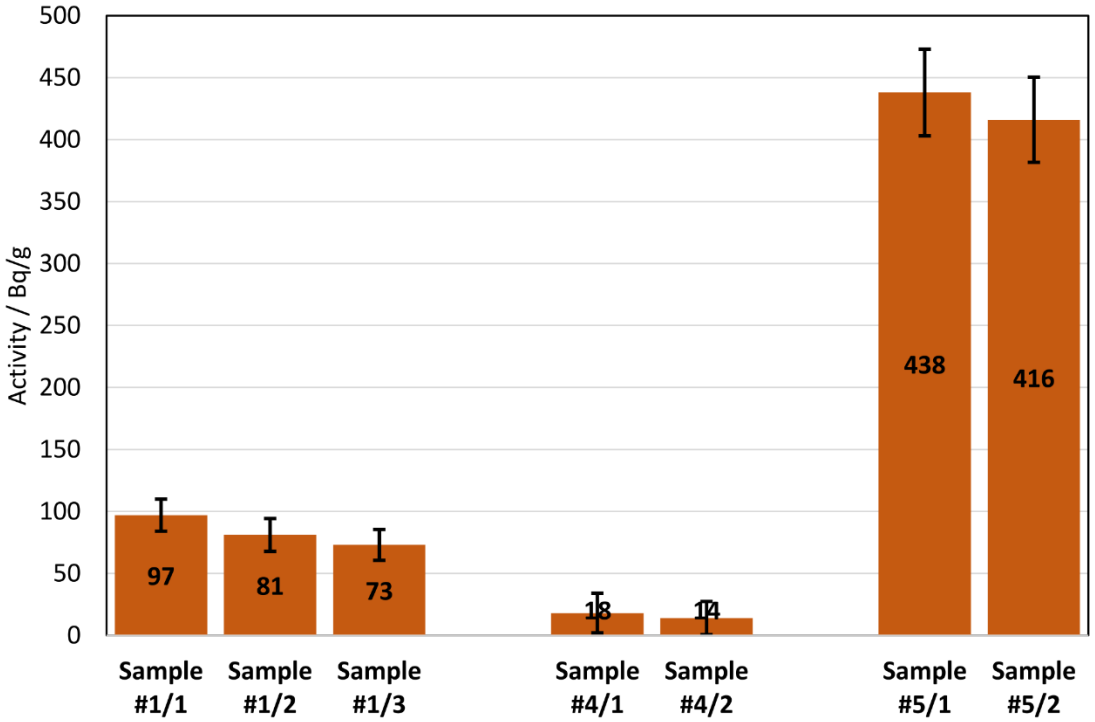

Figure 11. Activities in the irradiated graphite samples. Three measurements were done from sample #1 and two measurements were done from each of the samples #4 and #5. The measured ^{14}C activities in Bq/g are shown on the columns and the error bars are shown on the top of the columns.

There is little variation between the measured ^{14}C activity concentration within single samples. The variation is mostly due to variation of the actual activity within the graphite, which depends on the location on the graphite block. In addition, the distance from the graphite block surface affects the activity, as the radiation is strongest at the surface.

The ^{14}C activities measured with CRDS were clearly less than what was measured with liquid scintillation counting (LSC) 15 months earlier. The average ^{14}C activity of CRDS measurement from sample #1 was 84 Bq/g, while the activity from LSC measurement was 196 Bq/g, so about double the CRDS value. For sample #4, the CRDS average was 16 Bq/g and the LSC measured activity was 19.9 Bq/g, so the difference was smaller. For the most active sample the difference between CRDS and LSC measurement was the highest: 427 Bq/g compared to 1571 Bq/g, respectively. There can be a few possible reasons for the difference. One is that during the time between the LSC and CRDS measurements, there has been enough time for isotope exchange to occur between the graphite samples and surrounding air, which has lowered the ^{14}C activity in the graphite. The isotope exchange in carbon species has been studied earlier, and it was found to depend on the temperature [11]. Another explanation can be in the calibration of the CRDS measurement, which though should still be trustworthy in the ^{14}C activity concentration of the sample #1, but more uncertainty is present at the activity of sample # 5. Further investigations are necessary to determine the reason for this discrepancy.

The pyrolyser experiments with lower final sample zone temperatures resulted in more constant CO_2 output from the graphite, but also higher ^{14}C activity concentrations were detected with CRDS than with complete combustion. The experiments were done on the sample #5, which had the highest ^{14}C activity concentration. The CO_2 output from the graphite sample is shown in the Figure 12 b, where 16.6 mg of the sample was heated gradually with the pyrolyser from 500 °C to 680 °C and kept there. The CO_2 output started to decrease soon after the set temperature is reached. When stepwise heating 650°C – 660 °C – 670 °C was used to a sample of 17.2 mg as shown in Figure 12 a, the CO_2 output increased at every temperature step before it begun to decrease. The CO_2 output at these low temperatures was low, in general below 200 ppm. The low CO_2 concentration in trapping resulted in low pressure of about 2 mbar in the CRDS cavity after the release of the trapped CO_2. Two more experiments were done with larger sample sizes of 42 mg and 36.8 mg and with keeping constant sample temperature of 680 °C after gradual heating from 500 °C. The measured ^{14}C activity concentrations are shown in Figure 13 and the experiment details are explained below.

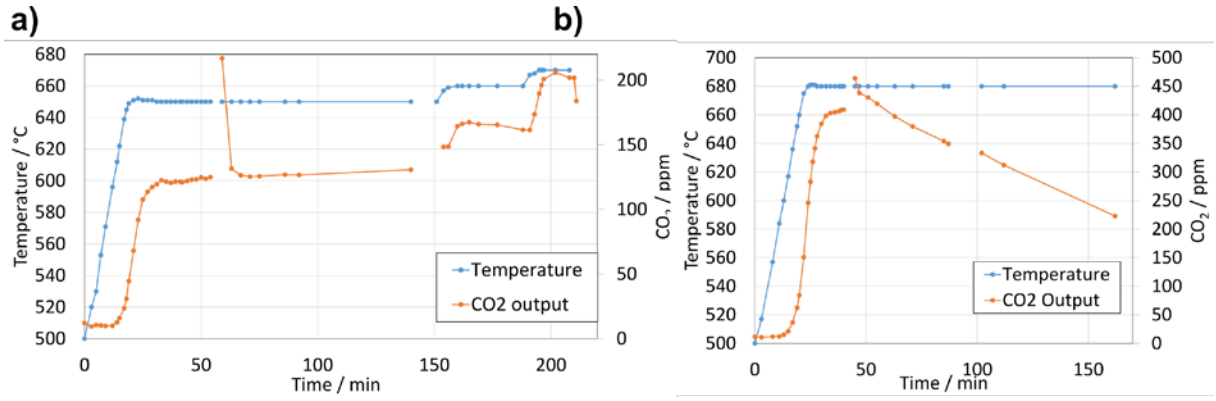

Figure 12. The development of CO_2 outgassing from graphite pieces with the pyrolyser temperature: **a)** stepwise heating the graphite resulted in slowly increasing CO_2 output, but at small rate; **b)** heating the sample directly to 680 °C and keeping it there resulted in fast increase to high CO_2 output followed by long decrease.

In combustion A (CO_2 output evolution in Figure 12a), 17.2 mg of sample #5 was set to the pyrolyser.

- In trapping A 1, the sample was heated from 500 °C to 650 °C in 18 minutes, but the trapping was continued for total duration of 41 minutes.
- In trapping A 2, the temperature was maintained at 650 °C and the trapping lasted for 81 minutes.
- In trapping A 3, the temperature was first increased from 650 °C to 660 °C in 9 minutes, maintained at 660 °C for 28 minutes, increased to 670 °C in 6 minutes and maintained there until the end of the measurement. The total duration of A 3 was 60 minutes and the final mass of the sample in the end of the experiment A was 7.5 mg.

In combustion B (CO_2 output evolution in Figure 12 b), 16.6 mg of sample #5 was set to pyrolyser.

- In trapping B 1, the sample was heated from 500 °C to 680 °C in 23 minutes and maintained at the end-temperature. The trapping time totalled 40 minutes.
- In trapping B 2, the sample temperature was maintained at 680 °C, and trapping was continued for 45 minutes.
- In trapping B 3, the sample temperature was kept at 680 °C and trapping took 71 minutes. 5.7 mg of the sample was left after the experiment B.

In combustion C: 42 mg of sample #5 was set to pyrolyser.

- The trapping C 1 was identical to trapping B 1.
- The trapping C 2 was the same as B 2, except that the duration was 47 minutes.

- The trapping C 3 was the same as the B3, but the duration was 70 minutes. The sample mass after the experiment was 25.6 mg.

In combustion D: 36.8 mg of sample #5 was set to the pyrolyser. The trapping sequence was the same as in B and C, but the trapping times were D 1: 45 minutes, D 2: 54 minutes and D 3: 71 minutes. The sample mass after the combustion was 9.8 mg.

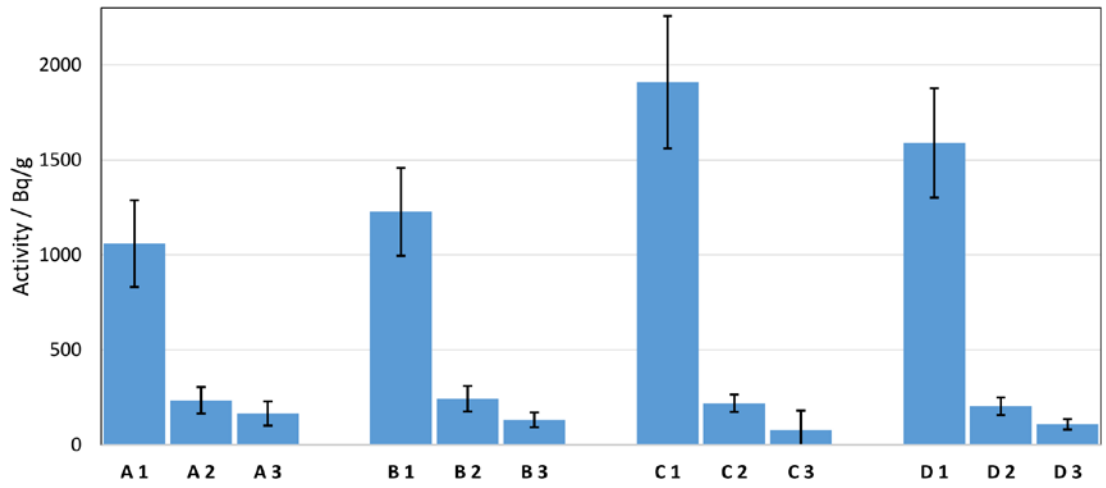

Figure 13. Measurements of the ^{14}C activity concentrations after long graphite combustion trapping.

The long combustion experiments at 650 – 680 C showed that the distribution of the ^{14}C in the graphite samples is not equal, but there is a gradient in the samples. The surface of the graphite and the surface of pores connected to the surface oxidise in the first combustion phase, and the highest ^{14}C activity concentrations were measured in A 1, B 1, C 1, and D 1. This is deduced based on the assumption that the $^{14}N(n,p)^{14}C$ is the main source ^{14}C in the graphite, and nitrogen from air can enter only the surfaces and pores that are connected with the surrounding air. The same surfaces and pores are also first available for oxygen in the beginning of combustion. The measured activities were clearly higher than what was measured from the complete combustion of the sample, and even higher than what was measured earlier with the LSC for the same sample. The highest activities were measured with the largest samples experimented, which also had the largest surface area. The measurements from the second and third phase trappings A 2&3, B 2&3, C 2&3 and D 2&3 show clearly lower and decreasing activity concentrations as the combustion propagated deeper into the graphite core.

4. Characterization of aged nuclear grade graphite using other methods

A characterization of nuclear grade graphite which has been preserved for more than 20 years under environmental conditions and exposed to air was also carried at ENEA laboratory using other methods than CRDS. This work complements the results presented above and provides additional information which can help in the understanding of ^{14}C outgassing from graphite waste. We are interested in verifying how properties, composition and chemical structure change due to aging and if these changes are important in aspects related to the disposal of nuclear waste in the final repository.

Graphite itself is a rather stable material and can only be altered by chemical attack with aggressive agents, such as concentrated potassium permanganate under very acidic conditions, highly concentrated hydrogen peroxide (> 30%) or ozone at high pressure and temperature. However, being exposed to the air for such a long time can have non-negligible effects. In particular, it could be expected that an alteration of the surface morphology could lead to a greater release into the environment under circumstances of substances trapped in the bars themselves, such as ^{14}C or ^{36}Cl. Nuclear grade graphite is manufactured to have a relatively high density, although it is inevitably lower than theoretical due to some degree of residual porosity. This porosity is mainly closed, therefore gas, air and other substances trapped in it can escape with difficulty. This is an advantage, from the point of view of the storage of nuclear waste. However, if there are phenomena that can lead to change this situation, they must be taken into consideration. Furthermore, the long aging these samples have been subjected to could simulate the situation to which other materials could be subjected to more aggressive conditions, such as strong neutron fluxes, intense heating, thermal shocks.

Figure 14 presents non irradiate graphite from ENEA laboratory, from which small pieces of graphite were cut and subject to combustion. Non irradiated aged graphite shown in Figure 14 was used to obtain some small cubes which were randomly selected from the graphite, as shown in Figure 15. Each small cube was analyzed using Raman analysis, SEM, and optical microscopy and to characterize their nitrogen content.

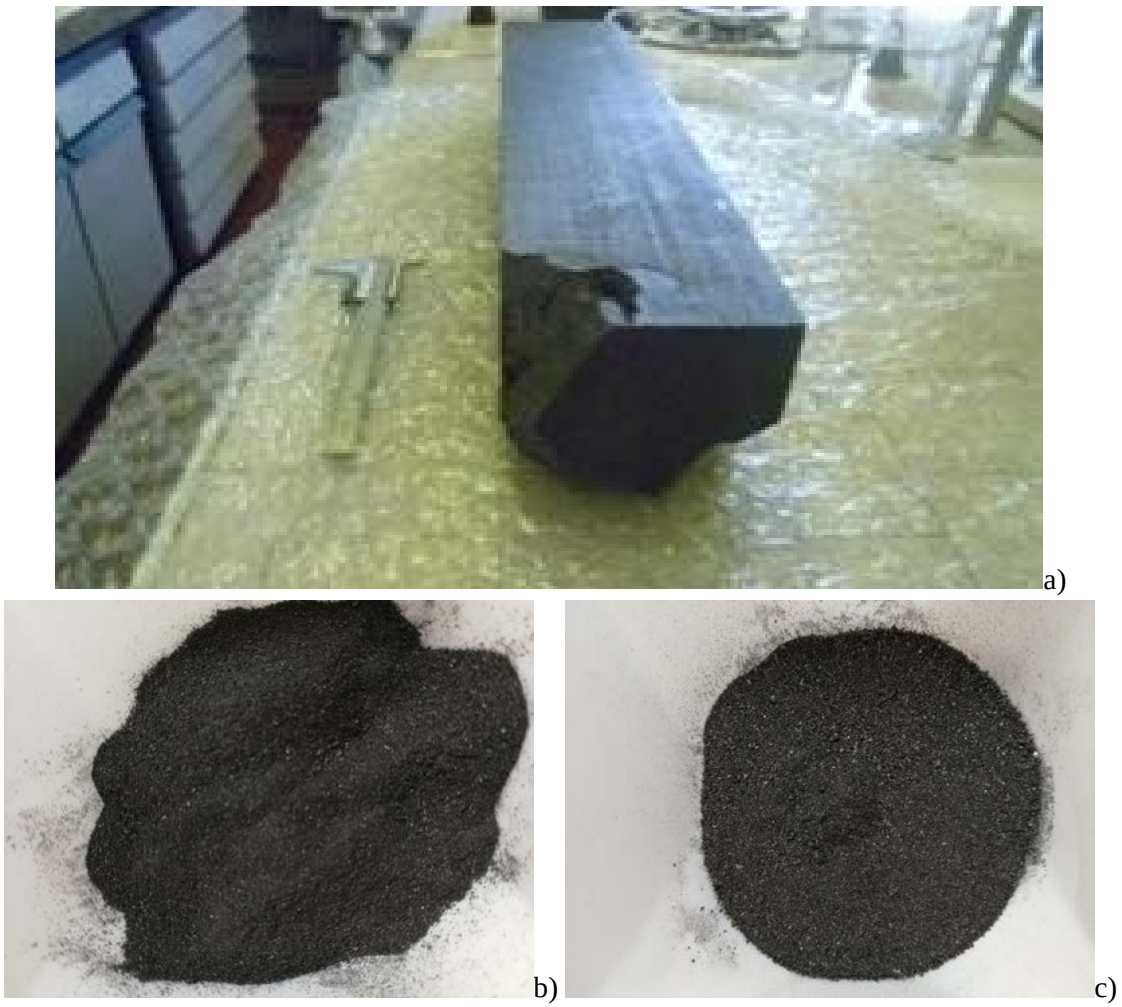

Figure 14. Non irradiated graphite analyzed at the ENEA research center: **a)** whole block of graphite; b) sand of graphite before combustion; **c)** sand of graphite after combustion.

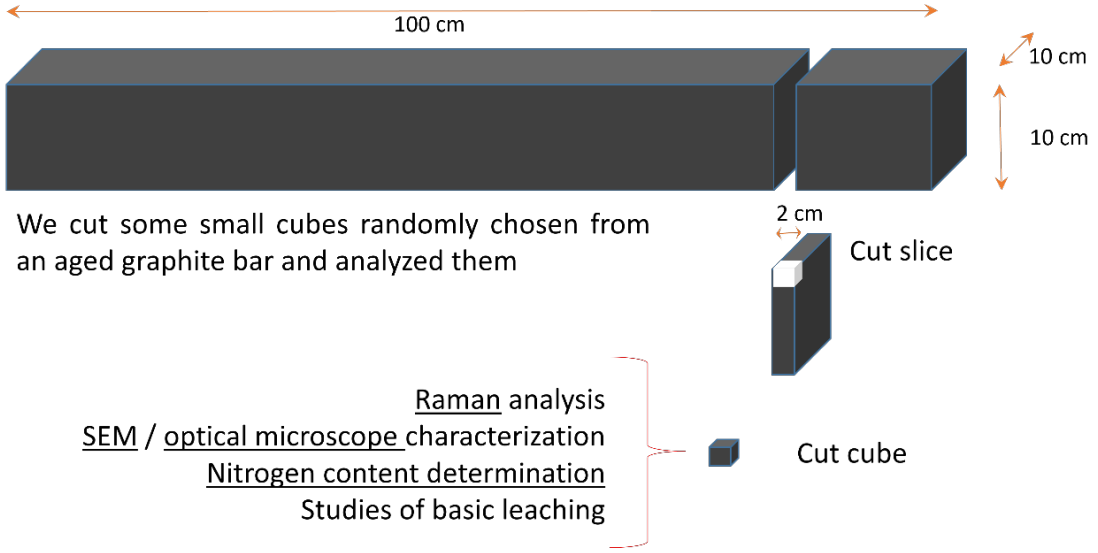

Figure 15. Graphical description of the procedure to obtain small pieces of graphite to analyze using different techniques.

4.1 Liquid Scintillation Counting analysis

The combustion system in the ENEA laboratory was optimized in order to oxide all the graphite content but to avoid the degradation of the carbonate content (Fig. 16).

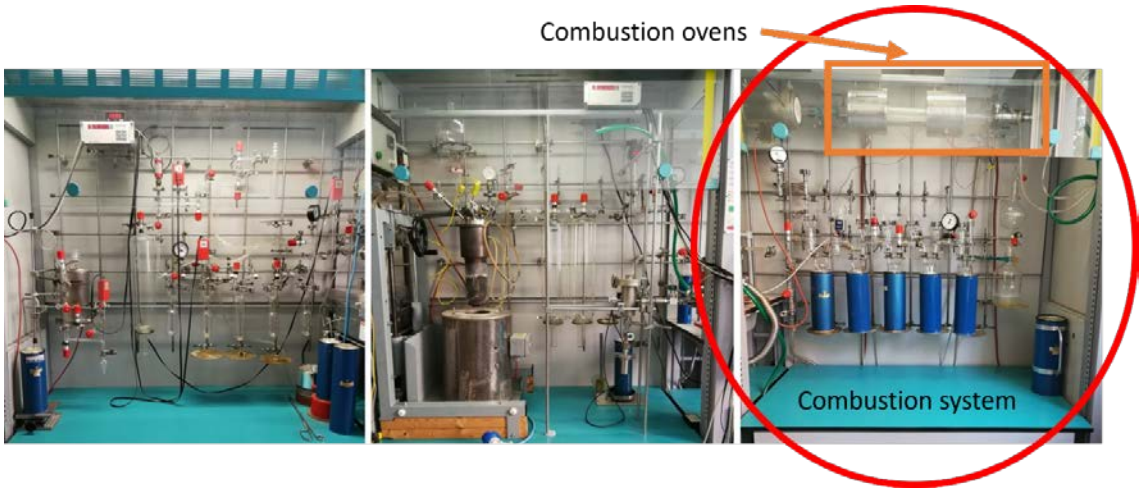

a)

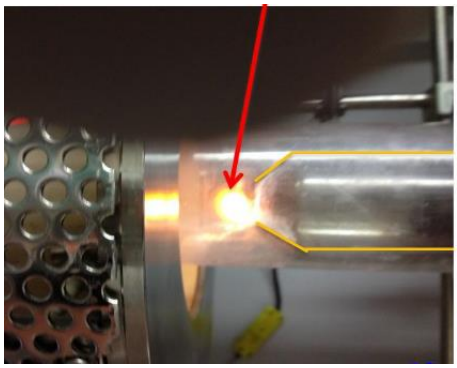

b)

Figure 16. Combustion system at the ENEA laboratory: **a)** complete combustion system; **b)** detail of the flame.

The system for CO_2 absorption and liquid scintillation counting (LSC) was designed and developed along with its measurement protocol for radiocarbon analysis in gaseous emissions. CO_2 is chemically trapped as a carbamate in a suitable absorbing solution (3-methoxy-propyl-amine), gravimetrically measured, and analyzed by LSC (using a Quantulus™ 1220) to determine the ^{14}C content.

In detail, the experimental apparatus is composed of a 5-L flask equipped with an inlet for gas storage, 4 cryogenic traps with different volume capacities (three 600-mL traps plus one 100-mL trap), a vacuum pump inlet, pressure transducer, and vacuum gauges, and a vial containing the absorbing solution (Figure 17). The flask collects and stores the CO_2 samples to be analyzed in sufficient amounts to ensure replicates of the analyses. The cryogenic traps in the system are designed to contain an excess amount of CO_2 to ensure a quantitative reaction with the absorbent present in the vial. The use of cryogenic traps and a pressure transducer in the system prevents the need for closed-loop recirculation or additional steps to maximize CO_2 capture in a short amount of time. The use of several stopcocks at different points

in the system permits different volume capacities depending on the amount of sample available and the progress of the reaction (about 2, 1.3, or 0.1 L, depending on the number of traps used).

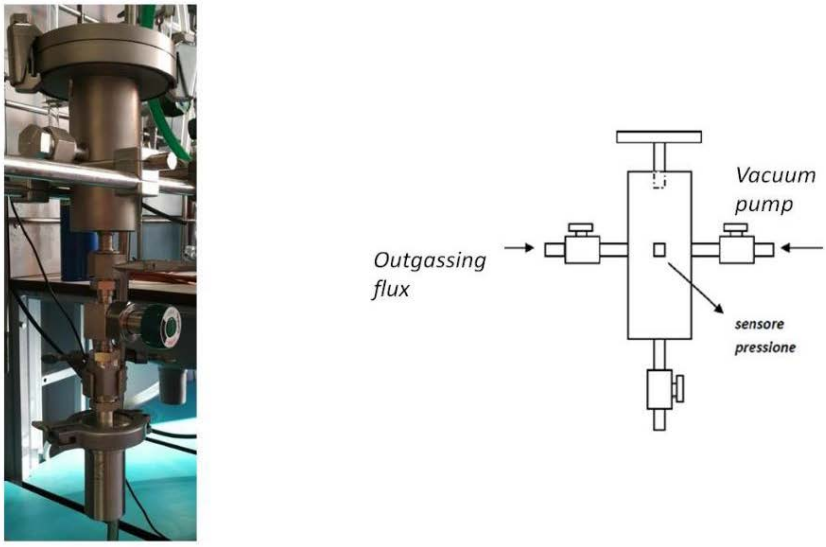

Figure 17. Equipment for the CO_2 direct absorption method [12].

With respect to conventional setups used in this field, the system was herein improved by adding a pressure transducer for monitoring the progress of the reaction in real time. A second upgrade is represented by the new CO_2 absorption cell. In particular, the vial was designed to fulfill the following requisites:

1. An optimized, air-tight fitting to the gas line setup by means of an internal thread so that it can be directly screwed to the end junction of the line;
2. Recovery of the vial after gas processing without any liquid transfer, i.e., LSC is carried out directly in the cell;
3. Use of PTFE for its fabrication to minimize instrumental background counting down to 40% with respect to the low 40K glass vials during LSC analysis

The vial contains an absorbing solution to chemically trap the CO_2. The sorbent used was the Carbo-Sorb E (PerkinElmer), a 3-methoxypropylamine, but no information about the degree of purity of the substance is provided. The PTFE vial is first filled with the absorbant and tightly closed under an inert atmosphere (argon) to minimize the possible risk of contamination by atmospheric CO_2. The CO_2 gaseous sample is collected into the system previously evacuated. A sufficient amount of CO_2, depending on the sample size, is then transferred and frozen by liquid nitrogen in the cryogenic traps to reach a pressure in the range of 1–1.4 bar, and finally it is allowed to sublime and react with the amine.

The system has been designed with an overall capacity (~7 L including the storage flask, or ~2 L with only the cryogenic traps and junctions) able to contain an excess of gas to ensure the complete conversion of CO_2 and amine into the carbamate at low pressure, avoiding security risks. Next, the vial is placed in an ice bath to reach the reaction equilibrium as well as to limit the loss of the volatile absorbant. The pressure transducers allow real-time monitoring of the reaction's progress. Amine saturation is achieved when the CO_2 pressure is stable. The absorption process takes about 15–20 min per sample.

At the end of the process, the vial is removed from the line and weighed to gravimetrically determine the amount of the absorbed CO_2 and the degree of saturation of the amine. The complete achievement of high-level saturation (greater than 80%) ensures easier and faster handling of the vial without requiring the use of a glovebox, as the risk of contamination is presumably very low because the reactive is mostly converted in a stable form. The sample of freshly formed carbamate in the PTFE vial is then combined with 10 mL of scintillator (Permafluor E+, PerkinElmer) and mixed with 2 mL of methanol (Carlo Erba, analytical grade) to prevent the risk of phase separation at a saturation level higher than 80%. The vial is then shaken and eventually sonicated to complete homogenization. The overall time required for each sample preparation is about 1 hr. The sample is finally counted for ^{14}C content determination by the Quantulus™ 1220 (PerkinElmer). The vial is stored for a few hours before counting in order to prevent chemiluminescence interference during ^{14}C counting.

4.2 Total carbon in the graphite samples

The total carbon content was determined by an elemental combustor, CN Vario Max Cube (Elementar). Figure 18 shows the total carbon content in the graphite samples from the reactor RB3. The ENEA RB3 reactor was a 100 Wth research installation owned and operated by ENEA, in its center of Montecuccolino near Bologna, from 1971 to 1989. Principal aim of the reactor was to provide neutronics data for the CIRENE NPP, a SGHWR that was being designed and then partially built in Latina starting from 1979. The specific RB3 core, surrounded by a graphite reflector and housed inside a concrete biological shielding, allowed to test easily very different fuel element configurations, In 1989, the RB3 reactor was shut down, and in the late 2010 ENEA received by ministerial decree the authorization to its dismantling, with the aim of reaching the "green field" status and with the unconditional release of its building, which is actually owned by the University of Bologna. The dismantling activities started in May 2013 and were concluded at the end of 2014; after that, a campaign for the radiological characterization of the building was initiated and concluded in June 2015.

The graphite samples come from the dismantling activity and were analysed for the purpose of CHANCE project. Some samples were not completely combusted by the process and some residues were collected for further analysis. The analysis shows that the residue samples have actually less total carbon than the original sample, but it means that the combustion process is not completed effectively even at higher temperature such as 600° C.

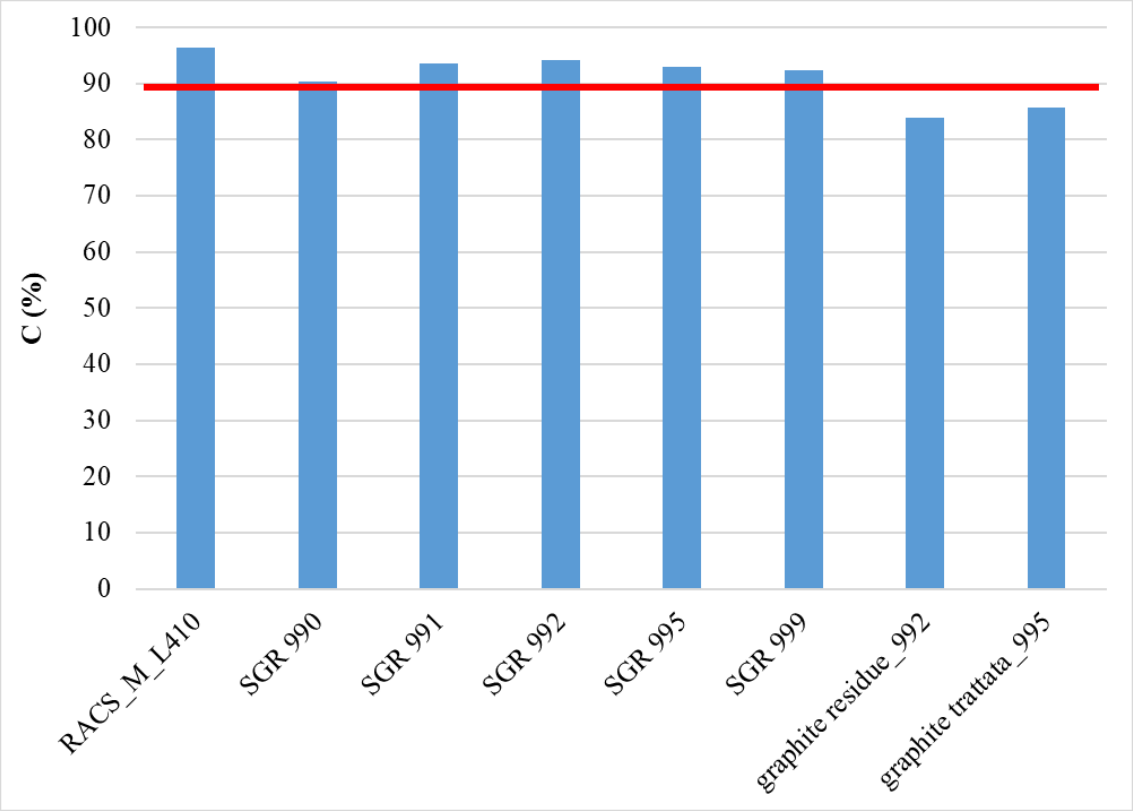

Figure 16. Total carbon content in the graphite samples from the reactor RB3.

4.3 Raman analysis

Raman spectroscopy analysis was also performed on several samples. Figure 19 shows a typical Raman spectrum performed in random points of the graphite from RB3. As the reactor has been shut down in 1989, this graphite was considered as naturally aged, also because they were stored in a closed container but not sealed. The experimental data was compared with the theoretical Raman spectrum of pure graphite and graphite oxide. The measurement conditions: laser power, acquisition times and other parameters have been chosen to minimize any possible effect on the samples due to the acquisition itself. In other words, an attempt was made to avoid the laser itself modifying the samples.

It can be noted that in many cases the spectrum obtained is very different from that of the theoretical graphite. The spectrum of the aged sample is more complicated than the spectra of the pure graphite or of pure graphite oxide, but it turns out to be a combination of the two.

Graphite has a band at about 2650 cm^{-1} that is the result of a high order process involving two phonons. This band is called the D band. It shifts to lower wavenumbers and becomes less intense as the number of crystalline layers decrease. It is still present in graphene, but it disappears in amorphous carbon and graphite oxide because of some selection rules. Therefore, it can be unambiguously attributed only to graphite in this case. The same band in the case of graphene would be at lower wavenumbers. Graphite oxide has two characteristic and rather wide bands in the region between about 1200 and 1600 cm^{-1}, which allow a fairly unambiguous identification of this material, although their exact location may depend on numerous factors, such as the degree of oxidation and the number of layers involved, which is difficult to estimate a priori. On the other hand, graphite has an extremely narrow and sharp Raman band for slightly higher wave numbers, at about 1580 cm^{-1}. Furthermore, graphite oxide is normally superficial, while graphite is found deeper and therefore the response of the former can be more intense also for this reason.

Graphite oxide is a chemical compound of carbon, oxygen, and hydrogen in variable ratios, normally obtained chemically by treating graphite with strong oxidizer. In the spectra of the analyzed samples, both signals can be identified even if their relative intensities can vary zone by zone due to the different Raman response of the two phases and due to their different relative quantity. This indicates the presence of both phases in many areas of the sample examined. In the insert of figure 19, this characteristic can be easily observed, since next to the broad band of the oxide, the narrow one of graphite is also evident. In other words, the final spectrum results from the combination of the two types of spectra, indicating the co-presence of two types of phases. it is difficult however to establish the relative ratio between them in the whole aged sample, because this ratio is not constant everywhere.

The relative abundance of oxide graphite compared to the pure graphite was estimated around 10-15 %. Graphite oxide is more abundant in the external layers, as illustrated in Figure 20.

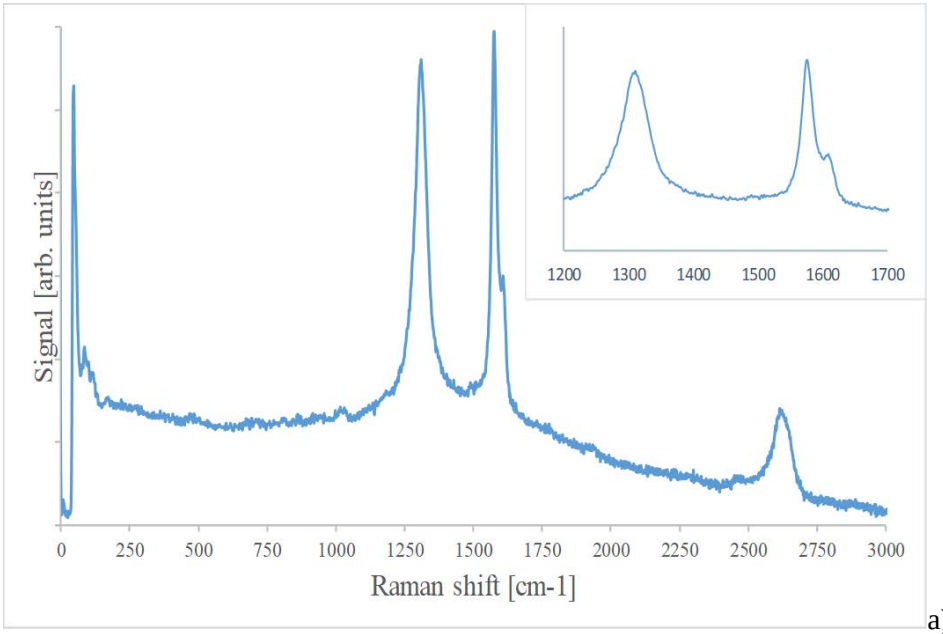

a)

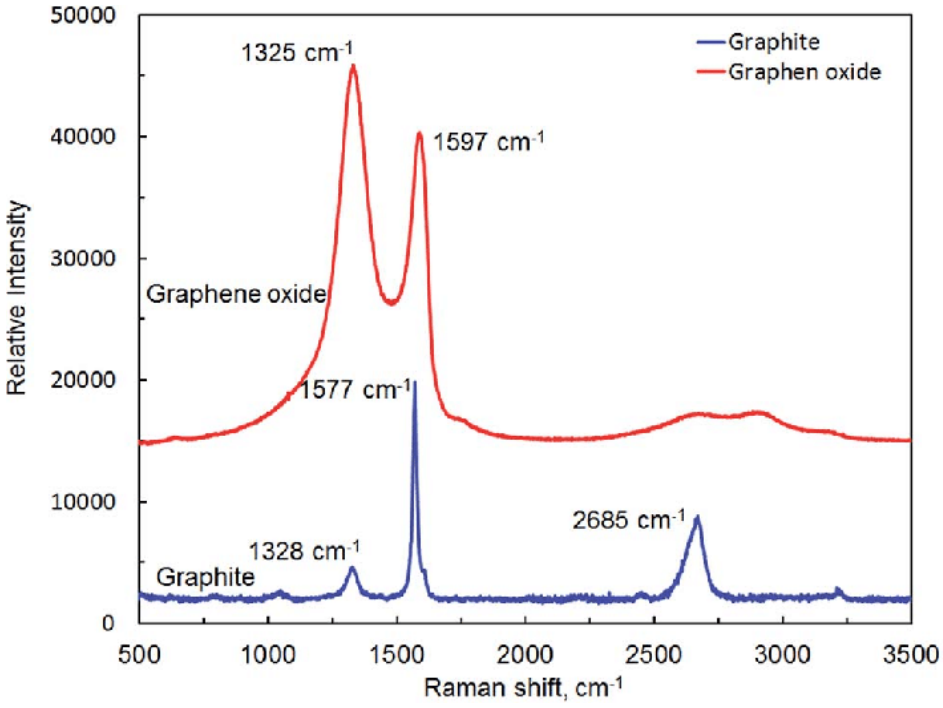

b)

Figure 17. Raman spectra: **a)** in a randomly chosen point of the aged graphite; **b)** theoretical Raman spectrum of pure graphite and graphite oxide [13].

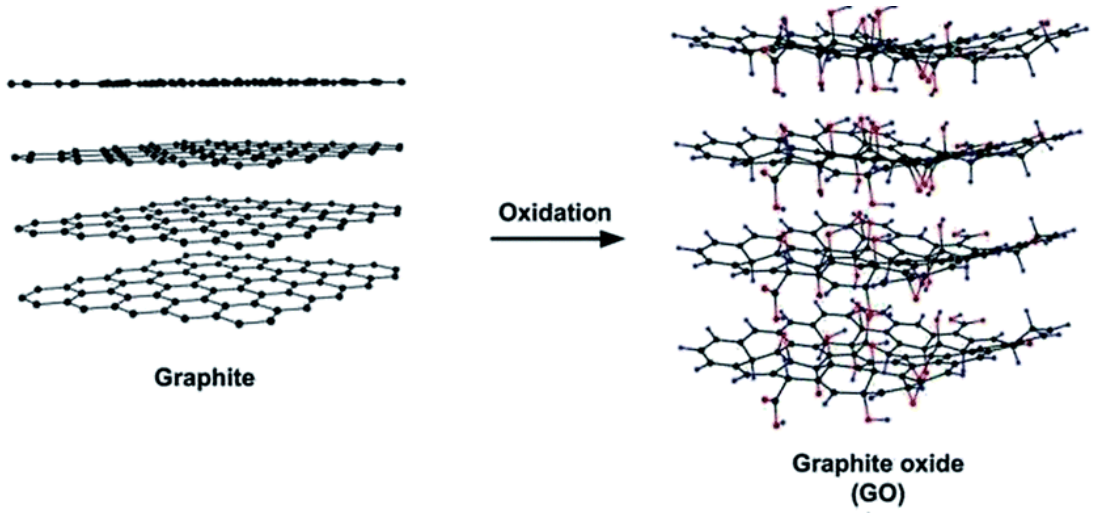

Figure 18. Illustration of the effect of oxidation on graphite [14].

The presence of graphite oxide can be explained by the oxidizing action of atmospheric oxygen over the long-term. Its concentration decreases moving towards the center of the bar and on the contrary, it is more abundant in the external part. This means that the reaction occurs by slow diffusion of oxygen from the outside towards the inside.

From a structural point of view, graphite is made up of layers of carbon atoms with hexagonal coordination within which there are very strong C-C bonds, held together by much weaker Van der Waals type bonds. For this reason, it is, in principle, possible to exfoliate a sample of graphite to obtain layers of monatomic thickness. They are called graphene and have exceptional physical and chemical properties and are the subject of enormous scientific and technological interest. However, on a practical level, exfoliation, particularly the spontaneous one, is not that simple and graphite remains stable over time. The situation is different in the case of the oxide, because the spacing between the planes increases and at the same time the interaxial bonding forces decrease. For this reason, exfoliation for this material is much easier and more spontaneous (the preparation of graphite oxide is chemically one of the methods of producing graphene). In this case, particles from the coffins can much more easily be released into the environment, resulting in serious contamination problems.

The substances and gases inside the graphite can also escape much more easily. Carbon and chlorine are very mobile atoms and can easily enter the chains of ecosystems. It is interesting to note that the nitrogen content in the samples is not constant along the section of the bars. It is rather low in the first layers, because, reasonably, it has already escaped from the porosity of the samples.

4.4 Structural characterization: SEM and optical microscope

The aged graphite was then analysed through Scanning Electron Microscopy (SEM) and optical microscopy to characterize its structure. Figure 21a shows the structure of the graphite using optical microscope and Figure 21b SEM picture of aged graphite.

Nuclear grade graphite has a porous structure; therefore, it can capture air, as it can be observed on the images. Moreover, the distance between the layers in the graphite oxide is greater than the pure one, favouring further absorption.

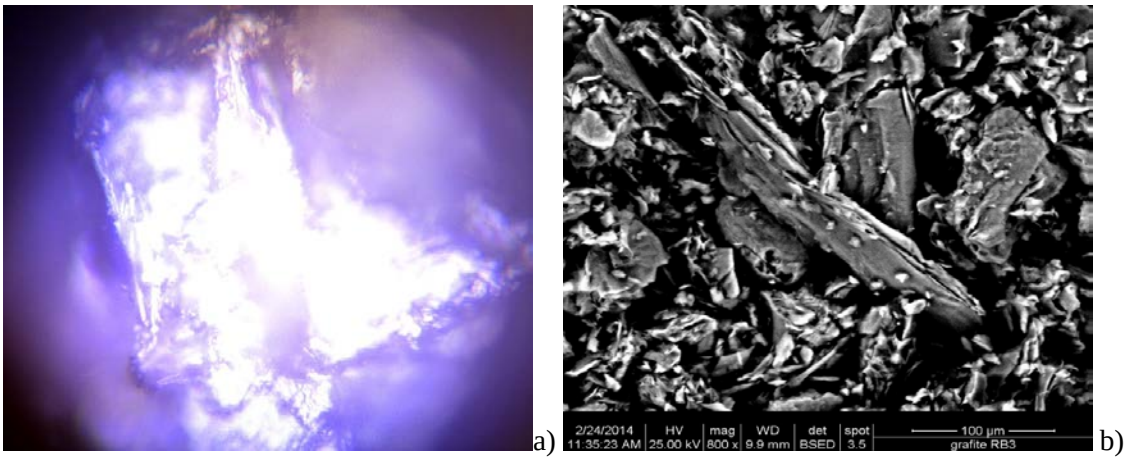

a) b)

Figure 19. Structure of the aged graphite obtained by using: **a)** optical microscope; **b)** scanning electron microscope.

4.5 Nitrogen content

Finally, nitrogen content of several graphite samples was determined by an elemental combustor, CN Vario Max Cube (Elementar). The samples were the same as the ones used for the analyses presented earlier (C14 and total carbon analysis, and Raman spectroscopy). For this analysis, two subsamples, were used, one from the internal core and one from the external layer. Some samples showed values close to the detection limit of the instrumentation, but others exhibit Nitrogen content up to 400 ppm, as shown in Figure 22b. This result is interesting because the nitrogen present, in some samples, could be not negligible and implies that during the reactor operation a not negligible quantity of radiocarbon can be formed, weakly bound. This aspect must be taken into consideration from the point of view of the final disposal.

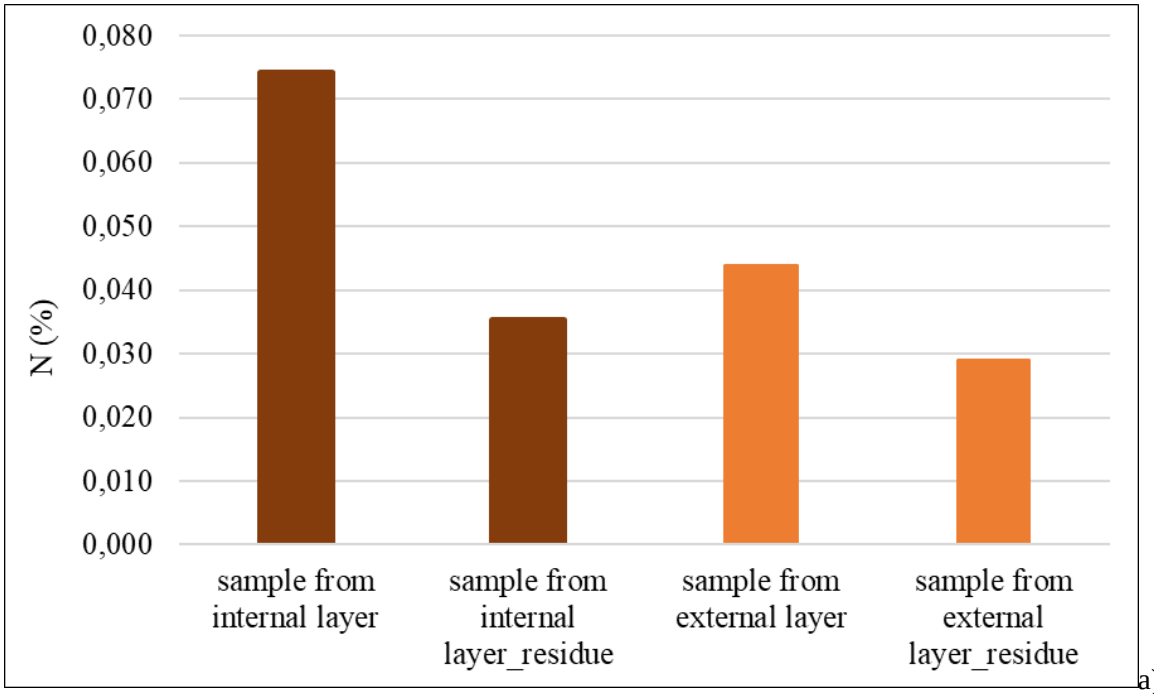

a)

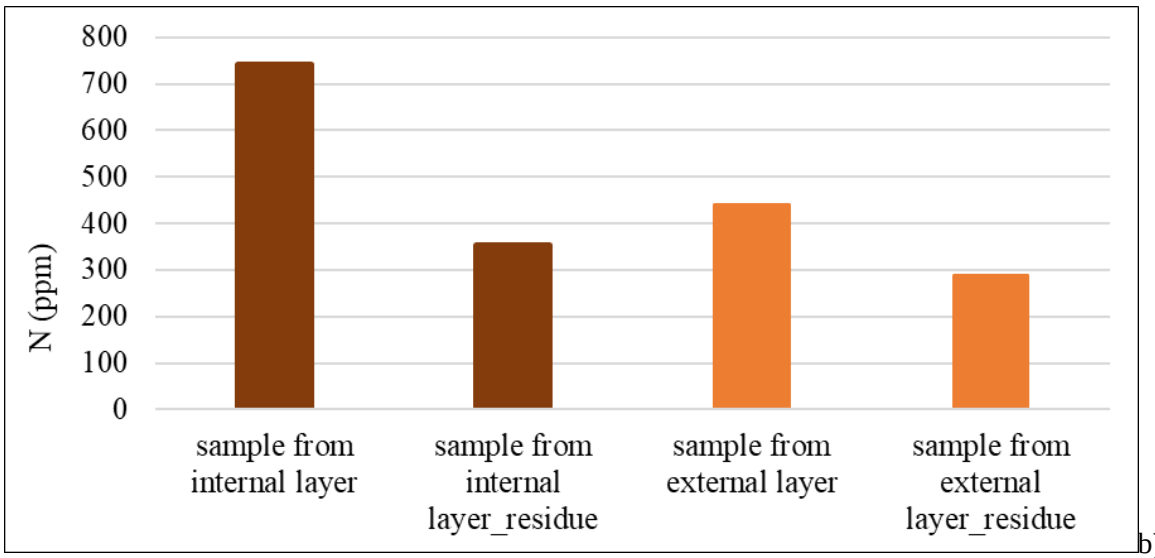

b)

Figure 20. Nitrogen content of some pieces of graphite: **a)** expressed in percentage; **b)** expressed in ppm.

4.6 Leaching test

In order to determine the amount of carbon that can be released from graphite, it was determined the ^{13}C content present in an isolated atmosphere in a leaching test chamber by injection of a known volume in a CRDS (Los Gatos research Inc.). Graphite samples was immersed in 100 ml of 1N NaOH and saturated, at different temperatures: -5 °C, 25 °C, 50 °C for different times: 2 days, 7 days, 15 days, 30 days.

Preliminary results indicate a greater presence of ^{13}C in the atmosphere of the samples treated at high temperature, increasing with the residence time in contact with NaOH, whose concentration plays a minor role. High basic conditions and temperatures higher than room temperature could in some cases simulate the conditions of the repository.

The idea behind this experiment is that under these experimental conditions, a small amount of carbon can migrate from the graphite samples to the leaching solution. Subsequently, a balance can be established between the carbon thus released and the atmosphere of the container. The higher the ^{13}C content released, the greater the amount of CO_2 containing it that can be formed. This can be measured as $\delta^{13}C$, with:

$$\delta^{13}C = \left(\frac{\left(^{13}C/^{12}C\right)_{camp} - \left(^{13}C/^{12}C\right)_{std}}{\left(^{13}C/^{12}C\right)_{std}} \right) 1000 \quad ‰$$

^{13}C can be considered, within certain limits and assumptions, a valid emulator of ^{14}C, because both have a mass greater than that of the more abundant stable isotope, 12C. The physical, chemical and biochemical processes they undergo are similar although not identical. Therefore it can be assumed that there is a similar partition phenomenon for these two isotopes. For example, the concentration of ^{13}C is used to estimate the ^{14}C concentration in organic carbon in atmospheric aerosols[15] [Elena N Kirillova, Rebecca J Sheesley, August Andersson, Örjan Gustafsson, nal. Chem. 2010, 82, 19, 7973–7978].

In this context, measuring ^{13}C in the outgassed CO_2 provides a valid indication of the physical occurrence of the process responsible of the outgassing, so it can be used to study the release mechanism and the parameters that could influence it.

The first results, although still preliminary, seem to indicate that temperature plays an important role in the release of ^{13}C.

In general, under these experimental conditions, the amount of ^{13}C increases with the leaching time (Fig. 23). Furthermore, for the same time, the higher the temperature, the greater the quantity of this isotope which enriches the leaching solution and consequently the atmosphere in the container. The following figure shows these first results.

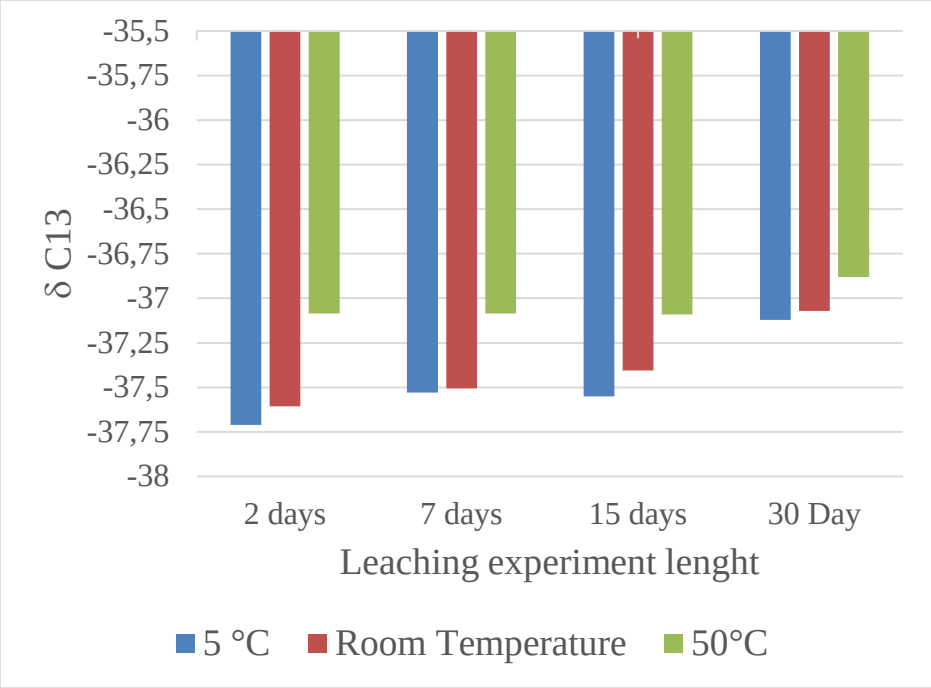

Figure 23. Trend of $\delta^{13}C$ as a function of time and temperature.

To investigate these results further, we have designed a measuring chamber that can allow analysis of both gas and liquid, shown schematically in Figure 24. This can be a further problem, due to the possible high mobility of the microflakes in the air.

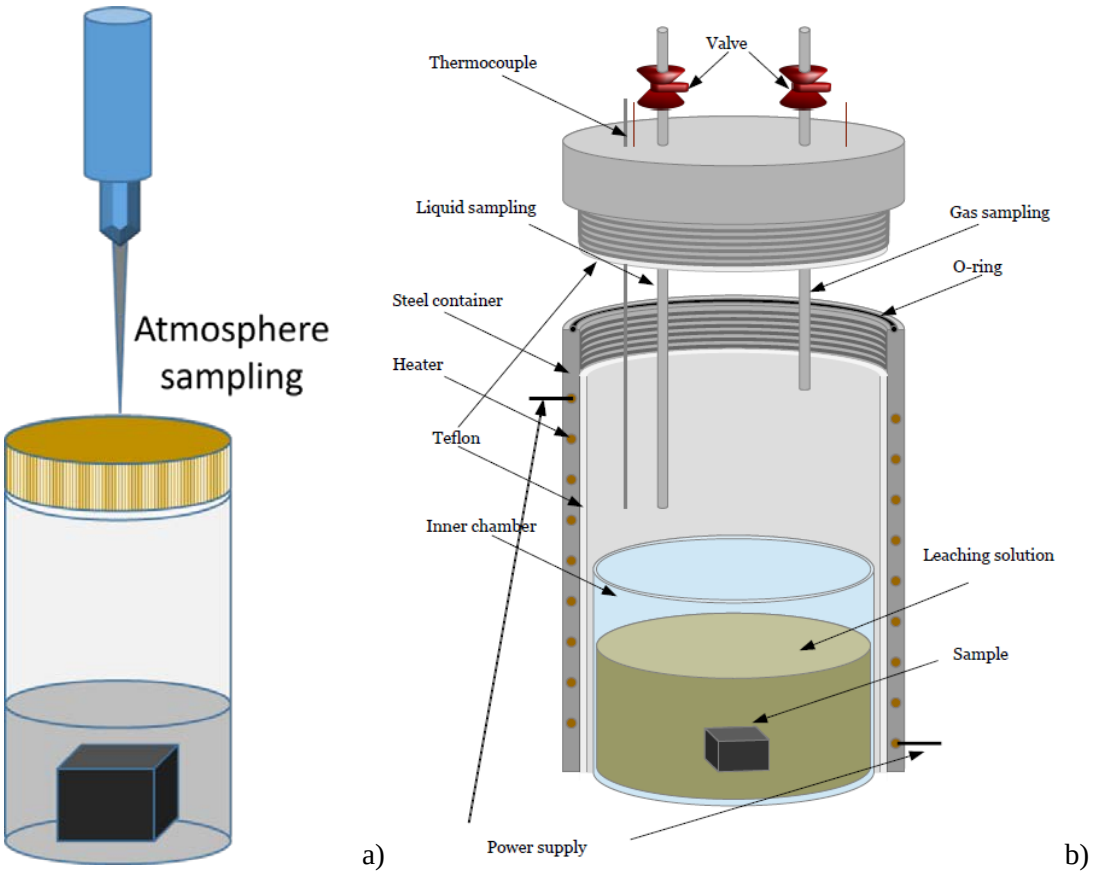

Figure 21. Experimental apparatus used for the analysis of outgas: **a)** simpler one; **b)** right more sophisticated.

5. Conclusions

The implementation of CRDS method in measuring outgassing of ^{14}C from graphite was demonstrated successfully. The measurements showed good repeatability and accuracy. The results were in line with the ^{14}C activities calculated based on $^{14}C/^{152}Eu$ ratio and the LSC measurements from the same samples, even though with the other methods, samples in the same exact state were not possible to measure.

New information could be gathered on the nature of ^{14}C outgassing from graphite. The mixing of the ^{14}C in different carbon containing species in air was successfully investigated from the stored graphite crates. This was possible because the method could detect the ^{14}C in different molecular species separately.

The distribution of ^{14}C in graphite was possible to examine by connecting the CRDS with the pyrolyser, which emphasises the flexibility of the operation of the CRDS. By combusting the graphite at different temperatures, the CO_2 outgassing was done in controlled manner. From single sample, the ^{14}C concentration could be detected at different depths of the sample, and a gradient in the ^{14}C distribution was discovered.

Further investigations carried out using other methods such as Scanning Electron Microscopy (SEM) and optical microscopy RAMAN, STEM and LSC provided more insight into how properties, composition and chemical structure of graphite change due to aging. This will provide insight to better understand the results from the CRDS measurements and whether these changes are important in aspects related to the disposal of nuclear waste in the final repository.

6. References

(1) Pageot, J.; Rouzaud, J.-N.; Gosmain, L.; Deldicque, D.; Comte, J.; Ammar, M. R. Nanostructural Characterizations of Graphite Waste from French Gas-Cooled Nuclear Reactors and Links with 14C Inventory. Carbon N. Y. 2016, 105, 77–89. DOI: doi.org/10.1016/j.carbon.2016.04.024

(2) Mileeva, Z.; Ross, D. K.; King, S. M. A Study of the Porosity of Nuclear Graphite Using Small-Angle Neutron Scattering. Carbon N. Y. 2013, 64, 20–26. DOI: https://doi.org/10.1016/j.carbon.2013.06.030

(3) Lee, W. E.; Gilbert, M.; Murphy, S. T.; Grimes, R. W. Opportunities for Advanced Ceramics and Composites in the Nuclear Sector. J. Am. Ceram. Soc. 2013, 96 (7), 2005–2030. DOI: https://doi.org/10.1111/jace.12406

(4) Räty, A.; Lavonen, T.; Leskinen, A.; Likonen, J.; Postolache, C.; Fugaru, V.; Bubueanu, G.; Lungu, C.; Bucsa, A. Characterization Measurements of Fluental and Graphite in FiR1 TRIGA Research Reactor Decommissioning Waste. Nucl. Eng. Des. 2019, 353, 110198. DOI: 10.1016/j.nucengdes.2019.110198

(5) Simmons, J. H. W. Radiation Damage in Graphite, PERGAMON-ELSEVIER SCIENCE LTD, 1965

(6) Pageot, J.; Rouzaud, J.-N.; Gosmain, L.; Duhart-Barone, A.; Comte, J.; Deldicque, D. 14C Selective Extraction from French Graphite Nuclear Waste by CO2 Gasification. Prog. Nucl. Energy 2018, 105, 279–286. DOI: 10.1016/j.pnucene.2018.02.003

(7) Cleaver, J. D.; McCrory, S.; Smith, T. E.; Dunzik-Gougar, M. L. Chemical Characterization and Removal of C-14 from Irradiated Graphite-12010; 2012

(8) Lehmuskoski, J.; Vasama, H.; Hämäläinen, J.; Hokkinen, J.; Kärkelä, T.; Heiskanen, K.; Reinikainen, M.; Rautio, S.; Hirvelä, M.; Genoud, G. On-Line Monitoring of Radiocarbon Emissions in a Nuclear Facility with Cavity Ring-Down Spectroscopy. Anal. Chem. 2021, 93 (48), 16096–16104. DOI: 10.1021/acs.analchem.1c03814

(9) Genoud, G.; Lehmuskoski, J.; Bell, S.; Palonen, V.; Oinonen, M.; Koskinen-Soivi, M. L.; Reinikainen, M. Laser Spectroscopy for Monitoring of Radiocarbon in Atmospheric Samples. Anal. Chem. 2019, 91 (19), 12315–12320. DOI: 10.1021/acs.analchem.9b02496

(10) Räty, A.; Kekki, T.; Tanhua-Tyrkkö, M.; Lavonen, T.; Myllykylä, E. Preliminary Waste Characterization Measurements in FiR 1 TRIGA Research Reactor Decommissioning Project. Nucl. Technol. 2018, 203 (2), 205–220. DOI: 10.1080/00295450.2018.1445402

(11) Park, J. H.; Hong, W.; Park, G.; Sung, K. S. 14C/12C Variations of Samples Exposed in Air According to Carbon Structure and Air Temperature. Radiocarbon 2013, 55 (2), 593–598. DOI: 10.1017/S0033822200057738

(12) Canducci, C.; Bartolomei, P.; Magnani, G.; Rizzo, A.; Piccoli, A.; Tositti, L.; Esposito, M. Upgrade of the CO2 direct absorption method for low-level 14C liquid scintillation counting. Radiocarbon 2013, 55 (2-3), 260.267.

(13) Alhwaige, A. A.; Alhassan, S. M.; Katsiotis, M. S.; Ishida, H.; Qutubuddin, S. RSC Adv. 2015, 5, 92719-9273.

(14) Tripathi, S. N.; Rao, G. S. S.; Mathur, A. B.; Jasra, R. RSC Adv. 2017, 7, 23615–23632.

(15) Kirillova, E., Sheesley, R., Andersson, A., Gustafsson, O., Anal. Chem. 2010, 82, 19, 7973–7978.